What determines the spatial pattern in summer upwelling trends on the U.S. West Coast?

Hyodae Seo,[1] Kenneth H. Brink,[1] Clive E. Dorman,[2] Darko Koracin,[3] and Christopher A. Edwards[4]

Received 29 February 2012; revised 10 June 2012; accepted 12 June 2012; published 9 August 2012.

[1] Analysis of sea surface temperature (SST) from coastal buoys suggests that the summertime over-shelf water temperature off the U.S. West Coast has been declining during the past 30 years at an average rate of $-0.19°C$ decade^{-1}. This cooling trend manifests itself more strongly off south-central California than off Oregon and northern California. The variability and trend in the upwelling north of off San Francisco are positively correlated with those of the equatorward wind, indicating a role of offshore Ekman transport in the north. In contrast, Ekman pumping associated with wind stress curls better explains the stronger and statistically more significant cooling trend in the south. While the coast-wide variability and trend in SST are strongly correlated with those of large-scale modes of climate variability, they in general fail to explain the southward intensification of the trend in SST and wind stress curl. This result suggests that the local wind stress curl, often topographically forced, may have played a role in the upwelling trend pattern.

Citation: Seo, H., K. H. Brink, C. E. Dorman, D. Koracin, and C. A. Edwards (2012), What determines the spatial pattern in summer upwelling trends on the U.S. West Coast?, *J. Geophys. Res.*, *117*, C08012, doi:10.1029/2012JC008016.

1. Introduction

[2] The eastern boundaries of major oceans are often characterized by coastal upwelling, a significant process for marine ecosystem and ocean biogeochemistry. The dominant forcing for upwelling is the along-shore equatorward wind stress [e.g., *Huyer and Pattullo*, 1972; *Brink*, 1983; *Huyer*, 1983; *Largier et al.*, 2006], leading to a well-defined co-variability (i.e., a positive correlation in the Northern Hemisphere) in wind stress and SST over the shelf [e.g., *Beardsley et al.*, 1987; *Dever et al.*, 2006]. The associated wind stress curls near the major coastal promontories are important to alongshore currents [*Marchesiello et al.*, 2003] and upwelling through Ekman pumping [e.g., *Enriquez and Friehe*, 1995; *Pickett and Paduan*, 2003; *Capet et al.*, 2004].

[3] *Bakun* [1990] has suggested that the upwelling rate, as inferred from equatorward wind stress, has been intensified in these eastern boundary currents. It has been posited that this enhanced upwelling is caused by a strengthening of the land-sea thermal contrast as a result of elevated greenhouse gas concentrations, which warm the continents more rapidly than the oceans [*Sutton et al.*, 2007]. The associated cross-shore surface pressure gradient then enhances along-shore geostrophic wind and consequently offshore Ekman transport. This link between the intensification in the upwelling rate and global climate change has been widely accepted in the literature based on instrumental data [e.g., *Schwing and Mendelssohn*, 1997; *Mendelssohn and Schwing*, 2002; *Bograd et al.*, 2009; *García-Reyes and Largier*, 2010; *Foreman et al.*, 2011], geological records [e.g., *van Geen et al.*, 1992; *McGregor et al.*, 2007; *Leduc et al.*, 2010; *Gutiérrez et al.*, 2011], and numerical models [e.g., *Snyder et al.*, 2003, *Diffenbaugh et al.*, 2004; *Diffenbaugh*, 2005]. The modified upwelling then impacts the biological productivity in pelagic coastal ecosystems [e.g., *Rykaczewski and Checkley*, 2008; *Bakun and Weeks*, 2008; *Bakun et al.*, 2010].

[4] However, due to short data records for over-shelf (15–25 km) SST, it is difficult to distinguish the physical processes controlling the secular trend in near-coast SST from those that are due to large amplitude interannual to multidecadal variability. The SSTs off the U.S. West Coast vary coherently with the large-scale coupled ocean-atmosphere phenomena [e.g., *Trenberth and Hurrell*, 1994; *Mantua and Hare*, 2002; *Miller et al.*, 1994; *Schwing et al.*, 2002; *Mestas-Nuñez and Miller*, 2006; *Macías et al.*, 2012]. For example, a positive phase of Pacific Decadal Oscillation (PDO, the leading principal component of North Pacific SST variability [*Mantua et al.*, 1997]) and a negative phase of the North Pacific Gyre Oscillation (NPGO, the 2nd dominant mode of sea surface height variability in the Northeast Pacific Ocean [*Di Lorenzo et al.*, 2008]) are known

[1]Physical Oceanography Department, Woods Hole Oceanographic Institution, Woods Hole, Massachusetts, USA.
[2]Scripps Institution of Oceanography, University of California, San Diego, La Jolla, California, USA.
[3]Division of Atmospheric Sciences, Desert Research Institute, Reno, Nevada, USA.
[4]Ocean Sciences Department, University of California, Santa Cruz, California, USA.

Corresponding author: H. Seo, Physical Oceanography Department, Woods Hole Oceanographic Institution, 266 Woods Hole Rd., MS 21, Woods Hole, MA 02543, USA. (hseo@whoi.edu)

0148-0227/12/2012JC008016

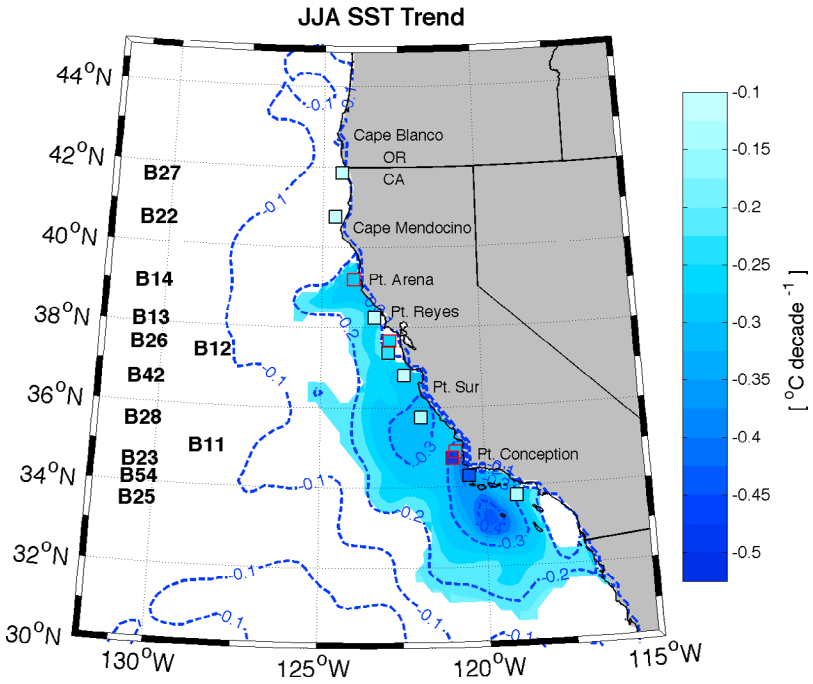

Figure 1. JJA SST trends in NOAA SST (contours, shaded if significant, [°C decade^{-1}]) in 1982–2010, overlaid with those from 12 NDBC buoys (squares). The buoy number (460##) is denoted on the left. Four buoys marked with red squares have significant trends in SST. The time series in SST and near-surface meridional wind from these 4 buoys are shown in Figure 2.

to be associated with an anomalously warm coast-wide SST. Thus, if only the past 30-year period (1980–2010) is considered, during which the PDO (NPGO) index has a significant negative (positive) trend (Section 5 and Figure 6), the coast-wide SSTs coherent with these modes of climate variability would show a multidecadal cooling trend [e.g., *García-Reyes and Largier*, 2010]. What is not clear is how correlation with such large-scale indices explains mechanistically what local processes are responsible for the observed spatial pattern in trends.

[5] The main objective of this study is to look for observational evidence for interlocking physical processes controlling the trend and its spatial pattern in the nearshore SST off the U.S. West Coast, using the 30-yearlong in situ and high-resolution gridded data. The trend referred hereinafter applies only to 1980–2010, a period with a strong negative (positive) PDO (NPGO) trend. We are not in a position to attribute the 30-year trend to any anthropogenic effect; this would require a long-term high-resolution modeling study in the future.

[6] The paper is organized as follows. Section 2 describes the data sets analyzed in the study. Section 3 reports the spatial pattern in the coastal upwelling trend, followed by an analysis of coastal wind and wind stress curl in Section 4. Section 5 explores the extent to which the trend and variability of upwelling SST are associated with the major modes of climate variability. Section 6 is a summary and discussion of implications.

2. Data Sets and Processing

[7] Moored over the continental shelf 15–25 km offshore over a range of West Coast locations (Figure 1), the coastal National Data Buoy Center (NDBC) buoys (http://www.ndbc.noaa.gov) record hourly near-surface wind (typically at 5 m height), air pressure (sea level), air temperature (4 m height) and water temperature (0.6 m depth) since the 1980s [*Hamilton*, 1980] (Table 1). In this study, the 0.6 m depth temperature is treated as an SST. The over-shelf buoy-measured SST is primarily controlled by upwelling [*Dorman and Winant*, 1995], and has been in fact used as a proxy for upwelling in previous studies [e.g., *Bograd et al.*, 2009; *Largier et al.*, 2006; *García-Reyes and Largier*, 2010]. Out of more than 26 moored buoys maintained by the NDBC off the U.S. West Coast, 12 were chosen that are located over continental shelves and have continuous records with gaps less than 35% of the boreal summer months (Table 1).

[8] To obtain a complete spatial pattern in SST, we also use the National Oceanic and Atmospheric Administration (NOAA) daily Optimum Interpolation (OI) of SST (hereafter NOAA SST, http://www.ncdc.noaa.gov/oa/climate/research/sst/oi-daily.php) [*Reynolds et al.*, 2007]. It incorporates the SSTs measured by the Advanced Very High Resolution Radiometer satellites with the in situ measurements obtained from ships and buoys based on the International Comprehensive Ocean–Atmosphere Data set [*Worley et al.*, 2005]. The relatively high resolution (25 km) and long-term (1981–2010) availability make NOAA SST a unique data set for studying near-coast SST. NOAA SST is highly coherent on interannual to multidecadal timescales with the NDBC buoy SSTs (Section 3), giving us confidence that it is a useful supplement to the buoy time series.

[9] For accurate analyses of trends in along-shore wind stress and its curl, one needs a high-accuracy long-term atmospheric reanalysis product that well resolves the fine-scale coastline and orography. There are few data sets that

Table 1. Information on the NDBC Buoys Listing the Location, the Years They Were Collecting Data in June–July–August, and the Percentage of Total Missing Hourly SST and Meridional Wind (VWND) Data for the JJA Period[a]

Buoys [NDBC 460##]	Locations	Years With JJA	Missing SST (%)	Missing VWND (%)	SST Trend	VWND Trends
B27	41.850 N 124.381 W	1983–2010	22	25	+0.05 ± 0.14	−0.13 ± 0.12
B22	40.776 N 124.589 W	1982–2010	19	14	−0.08 ± 0.16	+0.21 ± 0.27
B14	39.235 N 123.974 W	1981–2010	14	11	**−0.26** ± 0.12	+0.02 ± 0.09
B13	38.242 N 123.301 W	1981–2010	12	10	−0.06 ± 0.13	−0.07 ± 0.12
B26	37.759 N 122.833 W	1982–2010	16	12	**−0.25** ± 0.15	**−0.31** ± 0.09
B12	37.363 N 122.881 W	1980–2010	35	24	−0.23 ± 0.15	**−0.39** ± 0.10
B42	36.789 N 122.404 W	1987–2010	16	11	−0.02 ± 0.16	**−0.29** ± 0.12
B28	35.741 N 121.884 W	1983–2010	18	12	−0.12 ± 0.11	−0.21 ± 0.14
B11	35.000 N 120.992 W	1980–2010	13	13	**−0.30** ± 0.12	−0.07 ± 0.06
B23	34.714 N 120.967 W	1982–2010	5	6	**−0.48** ± 0.14	**+0.34** ± 0.13
B54	34.274 N 120.459 W	1994–2010	8	8	−0.41 ± 0.27	**+0.57** ± 0.26
B25	33.749 N 119.053 W	1982–2010	8	7	−0.13 ± 0.16	−0.01 ± 0.07

[a]The JJA linear trend with standard error in SST [°C decade^{-1}] and VWND anomalies [ms^{-1} decade^{-1}] at the 12 NDBC buoys are shown in the last two columns. Significant trends (90%) are marked in bold.

satisfy these requirements. In this study, we used the California Reanalysis Downscaling at 10 km system (hereafter referred to as CaRD10, http://cec.sdsc.edu [*Kanamitsu and Kanamaru*, 2007]), which is a dynamically downscaled analysis of the National Centers for Environmental Prediction (NCEP) / National Center for Atmospheric Research (NCAR) Reanalysis without data assimilation, but constrained via spectral nudging [e.g., *von Storch et al.*, 2000]. A lack of assimilation of the observed data in the CaRD10 analysis is nevertheless outweighed by its high spatial resolution information that much better resolves the effect of small-scale topography, which is essential for variability in the nearshore wind stress and curls. Indeed, the comprehensive validations of the downscaled wind fields over coastal oceans [*Kanamitsu and Kanamaru*, 2007; *Kanamaru and Kanamitsu*, 2007] show an improved agreement with the NDBC buoy observations on hourly to decadal time scales over the NCEP/NCAR Reanalysis as well as the North American Regional Reanalysis (NARR) [*Mesinger et al.*, 2006] with data assimilation on a 32 km grid. Given the high horizontal (10 km) and temporal (1 h) resolutions and the long-term availability (1948–2008), CaRD10 is suitable for assessing the multidecadal trend in the near-coast wind stress and curl [e.g., *Rykaczewski and Checkley*, 2008].

[10] The observed net surface heat flux (positive heating of the ocean) is obtained from the global Objectively Analyzed Air-Sea Fluxes (OAFlux) data set version 3 [*Yu and Weller*, 2007] for the period of 1983–2009 (http://oaflux.whoi.edu) on a 1° × 1° grid.

[11] Each daily or sub-daily data set is processed to calculate monthly averaged time series. For hourly buoy data, anomalies greater than three times the standard deviation are not used for subsequent monthly averaging. This quality-control procedure removes approximately 0.3% and 0.4% of the SST and meridional wind data, respectively. No month with more than 50% missing data is used for monthly averaging, which further eliminates approximately 17% and 15% of the total months. The climatological seasonal cycle is estimated based on the monthly averages at each buoy, and is subsequently removed to form interannual anomalies. If the resultant summer-mean (June, July and August, hereafter JJA) time series has missing values more than 35% of time, the corresponding buoy data is not used for this study. Finally, after 13 months' smoothing is applied to the monthly buoy time series, the JJA-mean linear trend is extracted. A linear trend was fit to each of these JJA time series using a robust multilinear regression over time [e.g., *Huber*, 1981]. It uses iteratively reweighted least squares with a bisquare weighting function [e.g., *Holland and Welsch*, 1977], which is particularly useful for data with gaps. Standard calculations of the statistical significance of the fitted trend were performed against the hypothesis of chance deviations from a flat trend. Unless noted otherwise, the 90% significance level was used. Correlations and regressions based on de-trended and normalized time series are also performed to assess the co-variability.

3. Trends and Variability of Coastal Upwelling

[12] Figure 1 shows the linear trends in JJA SST estimated from the 12 NDBC buoys (colored squares, Table 1), overlaid with the spatial pattern of the trend from NOAA SST (contours, and shaded if significant). Both data sets show summertime cooling along the entire Oregon-California coast since the 1980s. The averaged JJA SST trend over the 12 buoys is −0.19°C decade^{-1} (Table 2), which is broadly consistent with the NOAA SST trend sampled at the buoy locations (−0.26°C decade^{-1}). *García-Reyes and Largier* [2010], analyzing 11 NDBC buoys, also found a similar SST trend (an average of −0.22°C decade^{-1}). Assuming that this SST trend is all contributed by upwelling, they suggest that it is associated with stronger upwelling wind, more frequent occurrences of upwelling days, and lengthening of the upwelling season.

Table 2. Trends in JJA SST [°C decade^{-1}] and Meridional Component of Near-Surface Wind (VWND, Negative Equatorward, [ms^{-1} decade^{-1}]) Averaged Over all 12 Buoys, Northern 6 Buoys (from B27 to B12), and Southern 6 Buoys (from B42 to B25)[a]

	NOAA SST	Buoy SST	Buoy VWND	r(SST, VWND)
All 12 buoys	−0.26	−0.19	−0.03	0.16 (std = 0.33)
Northern 6 buoys	−0.19	−0.14	−0.11	0.30 (std = 0.29)
Southern 6 buoys	−0.32	−0.24	+0.06	0.02 (std = 0.33)

[a]The buoy-mean correlation coefficients (r) between the de-trended SST and VWND, and their standard deviations, are shown in the last column.

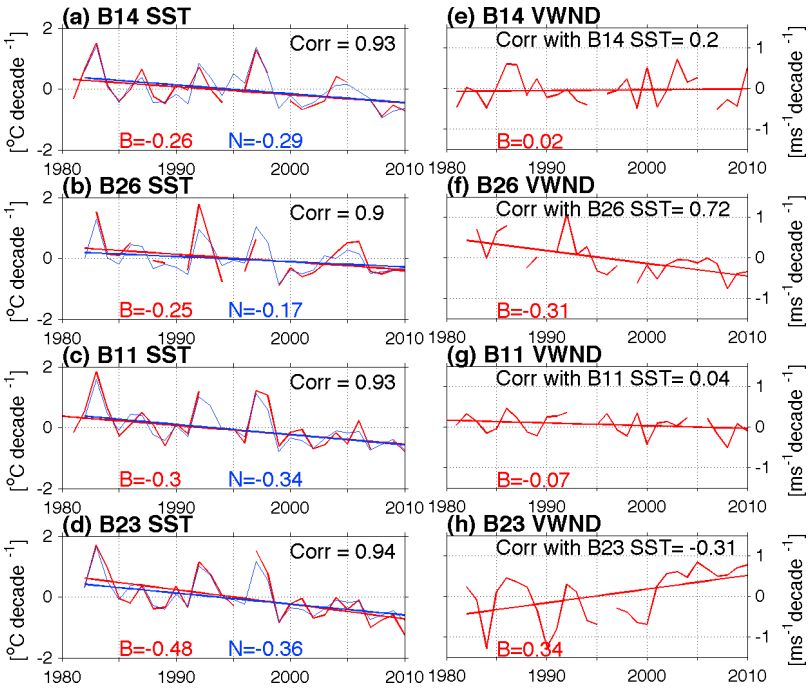

Figure 2. (a–d) JJA SST (red, [°C]) from 4 buoys marked in Figure 2a as red squares, overlaid with NOAA SST at the buoy locations (blue), and (e–h) corresponding meridional wind speed [m s^{-1}] (VWND). Trends (solid lines) in SST all are statistically significant at 90%, while those in VWND are significant only at B26 in Figure 2f and B23 in Figure 2h (Table 1). Correlation coefficients in the de-trended NOAA SST and de-trended buoy SST are shown in Figures 2a–2d. Also shown in Figures 2e–2h are the correlations between VWND and SST (both de-trended) at each buoy.

[13] Figure 1 also indicates that the cooling trend is greater south of central California than north of this region. A significant trend is only found from Pt. Arena (39°N) to beyond Pt. Conception, reaching 31°N. Within this area, the larger SST trends tend to be anchored to the sheltered side of major coastal capes, e.g., Pts. Arena, Sur and Conception. In particular, the zone of highest trend lies along 120°W in the lee of Pt. Conception extending into the Southern California Bight (SCB). The averaged trend increases substantially from the northern 6 buoys (−0.14°C $decade^{-1}$) to the southern 6 buoys (−0.24°C $decade^{-1}$). Averaging of NOAA SST at the buoy locations yields a greater contrast in trend magnitudes between the northern (−0.19°C $decade^{-1}$) and southern coasts (−0.32°C $decade^{-1}$, Table 2). According to NOAA SST, the maximum cooling trend is located off and in the lee of Pt. Conception (Figure 1). The next section explores the possible causes for this observed trend and pattern in coastal SST.

[14] Only four out of a total of 12 NDBC buoys analyzed here have a statistically significant trend in SST (Table 1). It is worth noting that, however, nearly all the buoys (except for B27), do show cooling trends [*García-Reyes and Largier*, 2010] consistent with the trend map from NOAA SST (Figure 1). A lack of significance in the large trend values summarized in Table 1 tends to be associated with lengthy gaps in the records (e.g., B12 compared to B26) and short data length (B54 compared to B23). Five buoys show significant trends in meridional wind (VWND, Table 1), three of which have upwelling-favorable trends around San Francisco in central California, while the other two have downwelling-favorable trends adjacent to Pt. Conception farther south (Table 1). Four buoys with significant trends in both SST, i.e., B14 off Pt. Arena, B26 off San Francisco, B11 off Santa Maria and B23 northwest of Pt. Arguello (these location are marked red in Figure 1), are shown in Figures 2a–2d). NOAA SST time series at these four buoy sites are also shown in blue curves. SSTs recorded from these buoys reveal strong interannual variability, which is highly correlated ($r > 0.90$) with NOAA SST. Both data sets also show clear downward trends in SST, with larger trends in the southern buoys than in the northern ones. B23 has nearly twice as large a trend (−0.48°C $decade^{-1}$) as B26 (−0.25°C $decade^{-1}$), which is also the case in NOAA SST.

[15] The same conclusion can be reached with the different measure of upwelling. *Nykjær and Van Camp* [1994] and *Narayan et al.* [2010] used the temperature difference between coastal water and water farther offshore at the same latitude as the index of coastal upwelling. With various choices of offshore distance (5° ∼ 20° longitudes), the upwelling estimate based on the NOAA SST data at the southern buoy locations tends to be stronger than those at the northern buoys by 135% to 200% (not shown), consistent with the results found by using SST alone.

[16] In summary, the analysis of over-shelf SST reveals a previously unidentified spatial pattern of coastal cooling trends; i.e., amid the well-observed multidecadal cooling trend of the U.S. West Coast in the past 30 years, there is also a tendency for a stronger trend in central-to-southern

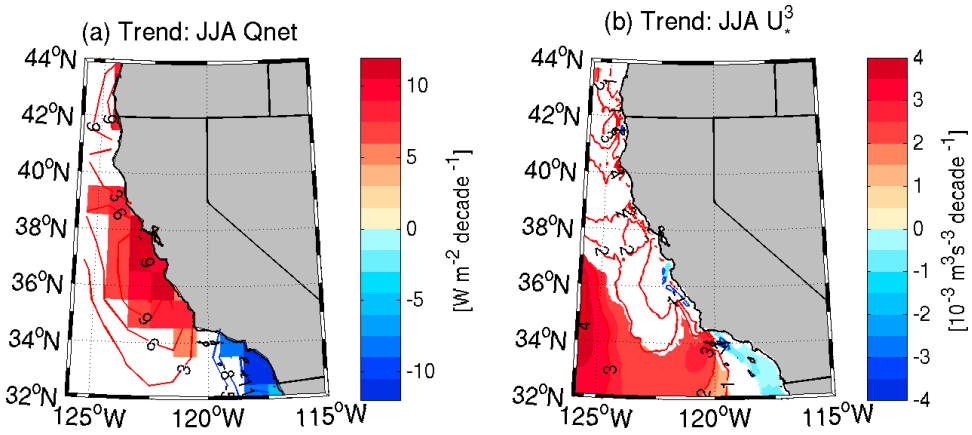

Figure 3. Trends (decade^{-1}) in JJA (a) net heat flux (Q_{net}, [W m^{-2}], positive into the ocean, shaded if significant, CI = 3) from the 1° × 1° OAFLUX (1983–2009) and (b) the atmospheric friction velocity cubed (U_*^3, [10^{-3} m^3 s^{-3}], CI = 1) estimated from 10 km CaRD10 10 m wind speed (1980–2008). Contours are shaded if significant.

California than in Oregon to northern California. What are the physical mechanisms for the observed SST trend, and what determines its spatial pattern?

4. Role of Ekman Transport and Pumping

[17] The regionally distinct covariability in wind-forcing and SST gives some insights into the dynamics responsible for the trend pattern. At the northern buoy B26, for example, JJA SST and VWND anomalies are highly, positively correlated (r = 0.72, Figure 2f), whereas the southern buoy B23 shows a negative correlation (r = −0.31, Figure 2h), indicating that the cold SST anomaly at B26 (B23) is associated with more equatorward (poleward) wind-forcing. In the area average sense, too, the northern 6 buoys tend to have a more positive correlation between SST and VWND (r = 0.3), while these are negligibly correlated (r = 0.02) in the southern 6 buoys (Table 2). The positive correlations in the northern buoys suggest that the observed SST trend and variability in the north are explained by the conventional description of coastal upwelling [e.g., *Huyer*, 1983], where the offshore Ekman transport is due to the equatorward wind-forcing [e.g., *Sverdrup*, 1937; *Yoshida*, 1955; *Smith*, 1968; *Pedlosky*, 1978]. B26 indeed shows significant trends toward upwelling-favorable, equatorward wind (−0.31 m s^{-1} decade^{-1}, Figure 2f) and colder SST (Figure 2b). Despite a much greater cooling trend (Figure 2d), in contrast, the southern location B23 features a downwelling-favorable, poleward wind trend (Figure 2h). This opposite sign in trends, together with the fact that SST and VWND are poorly correlated, implies that other mechanism(s) than offshore Ekman transport may be at work in driving a stronger SST trend in the southern buoys.

[18] How well would the surface heat flux and wind-induced mixing account for the observed spatial pattern in SST trend? Figure 3 shows two summertime trend maps for the net surface heat flux (Q_{net}) and friction velocity cubed (U_*^3, where $U_* = (\tau/\rho)^{1/2}$, where τ is the wind stress magnitude and ρ the density of air) extracted from 1° × 1° OAFLUX (1980–2009) and 10 km CaRD10 (1980–2008), respectively. Q_{net} has a significant positive trend around central California, favoring an increase, not a decrease, in coastal SST. A further decomposition of Q_{net} reveals that this warming effect is primarily driven by a decrease in latent heat loss, presumably over the increasingly colder water, with a minor contribution from decreased sensible heat loss (not shown). This suggests that Q_{net} is unlikely to cause the observed cooling trend. As for the wind-induced mixing, Figure 3b shows that U_*^3 has areas of maximum and minimum trends off southern California straddling the area of maximum SST trend along 120°W (Figure 3b). Although the role in mixing cannot be ruled out in the offshore region of the maximum SST trend at 120°W 33°N, the apparent shift in the pattern of SST trend with respect to that in U_*^3 also suggests a possible role of the trend in derivatives of wind stress, i.e., wind stress curls.

[19] As upwelling along the central-to-southern California coast is strongly controlled by wind stress curl [*Bakun and Nelson*, 1991; *Koračin et al.*, 2004; *Dorman and Koračin*, 2008], we ask if the significant trend in wind stress curl could come into play in the observed SST trend pattern. As the wind stress curl cannot be estimated confidently based on the buoy-measured wind stress, we instead focus on the CaRD10 model wind stress curls. Figure 4 shows the maps of trends in summertime wind stress and wind stress curls. All along the coast, the upwelling-favorable wind stress (reddish contours in Figure 4a and southeastward vectors in Figure 4b) has been intensified in 1980–2008, but far more significantly well offshore of southern California. In particular, the significant trend in southeastward wind stress in the lee of Pt. Conception seems to be critical in generating the region of the maximum positive trend in wind stress curl there, which then extends toward the SCB. Although not significant, the prevalent southeastward trends in wind stress between Cape Blanco and Cape Mendocino and from Pt. Sur through Pt. Conception (Figure 4b) are conducive to a significant positive nearshore curl due to a drop-off in the wind near the coast [*Capet et al.*, 2004]. For this reason, hydraulic flow features, often observed with an upwind compression bulge and a downwind expansion fan off the main capes [e.g., *Dorman*, 1985; *Winant et al.*, 1988; *Edwards et al.*, 2002], are manifested in the trend map. The spatial correspondence

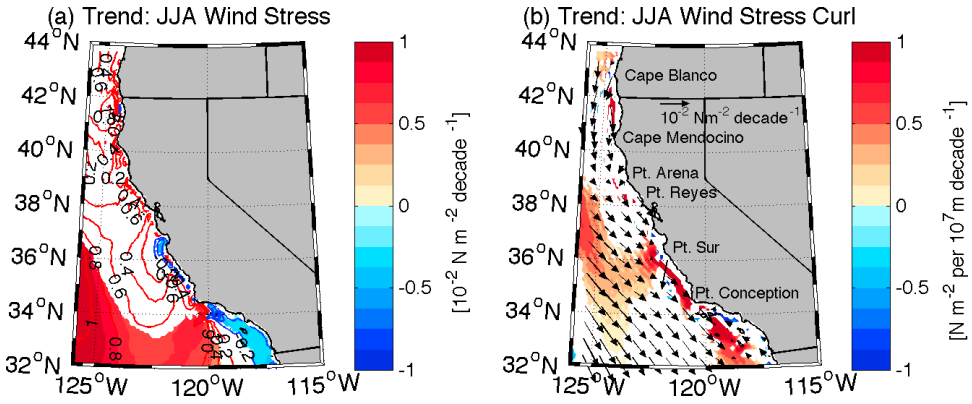

Figure 4. Trends in (a) CaRD10 JJA wind stress magnitude (contours, and shaded if significant, [10^{-2} N m^{-2} decade^{-1}], CI = 0.2) and (b) wind stress vectors (arrow lengths denoting the wind stress magnitudes) in 1980–2008. Figure 4b shows the trends in JJA wind stress curls (shaded, [N m^{-2} per 10^4 km decade^{-1}]). Shading in Figure 4b indicates the area of significant trend in wind stress curl, while the non-significant trends are not displayed for clarity. The reddish shades/contours in Figure 4a, along with the vectors in Figure 4b, denote the trend for upwelling favorable (southeastward) wind stress. Likewise, the negative trend (bluish shades/contours) off the central CA and SCB indicates the trend for less upwelling favorable (northwestward) wind stress. The lateral sponge layers (27 grid points, roughly 13% of the domain width) from the northern, southern, and western boundaries of the CaRD10 domain are not shown.

in the trends between wind stress curl and SST strongly implies the potentially important role of the wind stress curl in the pattern of upwelling trend through Ekman pumping.

[20] Since wind-driven upwelling is due to the along-coast wind stress and also the wind stress curl, which are limited to different geographical regions, can we quantify their relative roles in the identified trend pattern? The two factors are presented here side by side to examine if the trends in the two different processes are significant. In Figure 5, we calculate the latitudinal distributions of the JJA mean and trend of offshore volume transport (m^3 s^{-1} per 100 m coast) due to Ekman transport and Ekman pumping from the CaRD10 model, following the method by *Pickett and Paduan* [2003]. Ekman transport is computed as $EkT = (1/\rho_w f)\ \tau \times \hat{k}$, where τ is the summer-mean equatorward along-shore wind stress (ASW) estimated at the first three ocean grid points off the coast (the result is not sensitive to choice of grid points used), ρ_w the density of seawater, f the Coriolis parameter, and $\hat{k}$ the unit vertical vector. ASW is obtained by projecting coastal wind stress vectors parallel to the coast, an orientation obtained by fitting a straight line through a 50-km segment of coastline. We thus have the Ekman transport at every 10 km coastal grid point. The vertical transport by Ekman pumping is computed using $EkP = (1/\rho_w f)\ \nabla \times \tau$, which is then integrated over the cross-shelf distance d where the wind stress curls remain positive, which varies from 50 km in Cape Mendocino to 250 km in SCB. The use of a constant cross-shelf distance such as 200 km [*Pickett and Paduan*, 2003] or 300 km [*Castelao and Barth*, 2006] produces essentially the same result. The vertical transport estimated from the integrated Ekman pumping is also available at every coastal grid point and hence can be directly compared with the Ekman transport [e.g., *Castelao and Barth*, 2006].

[21] All along the coast, the integrated Ekman pumping tends to be comparable to or larger than the Ekman transport (Figures 5a and 5b). The relative magnitude and latitudinal distribution of both (shown in Figures 5a and 5b) are consistent with the analysis of both transports by *Pickett and Paduan* [2003] from a high-resolution atmospheric model. They suggested that the curl-driven Ekman pumping is larger than the Ekman transport all along the coast, except within the SCB where the upwelling transport is nearly entirely due to Ekman pumping. The peaks in the mean Ekman pumping tend to be located off the large coastal capes [*Koračin et al.*, 2004; *Dorman and Koračin*, 2008], hinting that they may be topographically forced.

[22] The trends for the computed wind driven upwelling by ASW and curl are both independently increasing north of Cape Mendocino, but mostly not significantly (Figures 5c and 5d). South of San Francisco (38°N), the greater and more significantly increasing trend is in the wind stress curl. The trends in Ekman pumping tend to peak downstream of the major topographic features. For example, the trend value in Ekman pumping doubles from 0.76 to 1.54 m^3 s^{-1} per 100 m from Pt. Conception (34.44°N) to 1° latitude southward. The trend over the entire coast by both aspects favors increased upwelling, which is consistent with other trends in the SST and winds.

5. Role of Large-Scale Modes of Climate Variability

[23] As discussed in the Introduction, the period of 1980–2010, during which the significant cooling trend in buoy and NOAA SST is observed, also corresponds to the period of strong negative (positive) trend in PDO (NPGO). Hence it is natural to ask if and how well such modes of climate variability correlate with the observed spatial structure in the SST trend. This is addressed in Figure 6, where the left column shows the normalized JJA mean PDO and NPGO indices. The PDO has a clear negative trend in 1980–2010 (Figure 6a), while the NPGO has an upward trend (Figure 6c). The right column of Figure 6 displays the corresponding simultaneous regression coefficients of JJA SST from NOAA SST data and

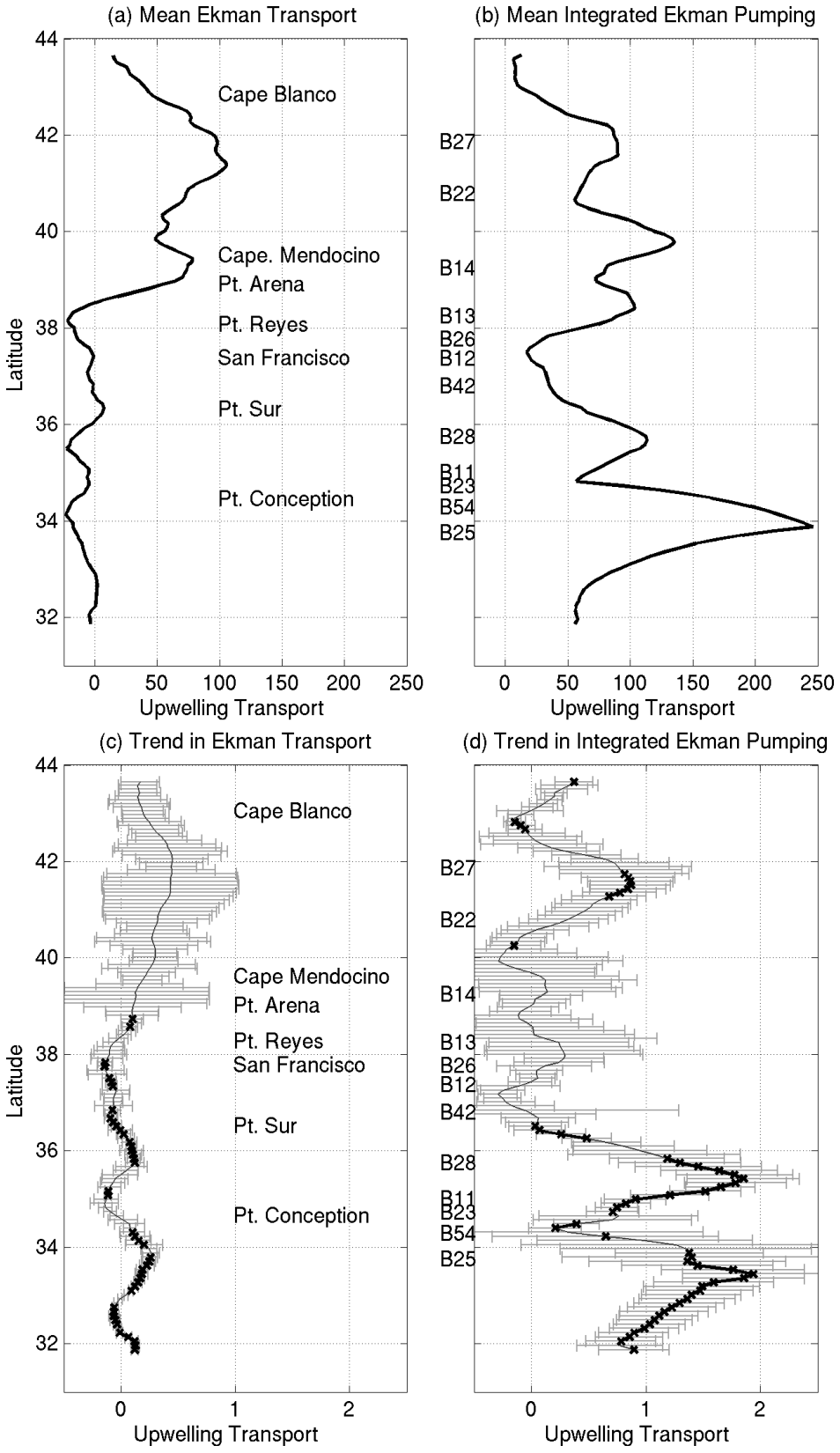

Figure 5. (a and b) Latitudinal distribution of JJA mean offshore volume transport [$m^3\ s^{-1}$ per 100 m of coast], and (c and d) the trend in 1980–2008 [$m^3\ s^{-1}$ per 100 m of coast $decade^{-1}$] by Ekman transport by alongshore wind stress (left column) and Ekman pumping by wind stress curl (right column). The trends that are statistically significant at 95% are marked with a thick cross. Standard error is shown in error bars for each coastal location.

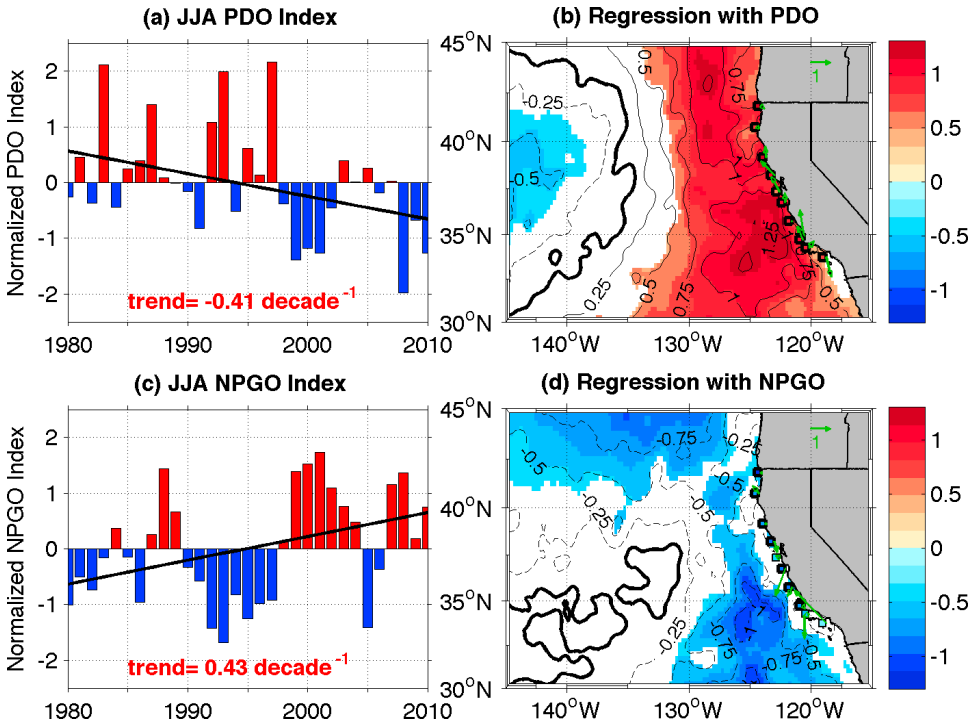

Figure 6. (a and c) Bar plots showing the normalized JJA PDO and NPGO index from 1980 to 2010. Overlaid are the linear trends (solid black lines) for 1980–2010. The respective trend values are displayed at the bottom of each panel (marked in red if significant). (b and d) Maps of regression coefficients in JJA SST [°C per unit index change] from NOAA SST (shaded) and from buoys (filled squares) against the PDO and NPGO index in 1980–2010. The zero contours are shown in thick black lines (CI = 0.25). The regression coefficients of the near-surface buoy winds [m s^{-1} per unit index change] are also shown in green vectors at each buoy location. Before regression, each variable is de-trended to remove the linear trends.

buoys. The regression coefficients of the measured surface winds at the buoys against each index are also displayed as green vectors. The time series are all de-trended prior to the regression analysis, so the regression coefficients multiplied by the trend of each index can be inferred as the portion of the total trend that is driven by large-scale climate patterns.

[24] As for PDO (Table 3), the U.S. West Coast SST anomalies exhibit the positive phase of the canonical PDO pattern resembling a horseshoe, with cold temperature anomalies in the central North Pacific surrounded by anomalously warm SST off California (Figure 6b). The positive PDO phase is generally associated with less upwelling-favorable wind (green vectors in Figure 6b), indicating that the near-coast warm SST anomalies are associated with the weaker upwelling condition [e.g., *Chhak and Di Lorenzo*, 2007]. Associated with NPGO, the California SST has negative regression coefficients coast-wide with, in general, equatorward alongshore winds at the buoys, indicating an upwelling-favorable condition when they are in a positive phase [e.g., *Chenillat et al.*, 2012]. The negative trend in PDO together with positive regression coefficients in SST, and also the positive trend in NPGO together with negative regression coefficients, suggest that the cooling trends observed at the west coast buoys in 1980–2010 are all strongly related to the climate modes of variability being considered. The coast-wide summertime SST trends, inferred as the product of area-averaged regression coefficients from buoys (Table 3) with the 1980–2010 trend of each index (Figure 6), all exhibit cooling trends of $-0.29 \sim -0.42$°C $decade^{-1}$ (Table 3), which is broadly consistent with the mean trend from buoys (Table 1).

[25] While the coast-wide SST trend is associated with the large-scale modes of climate variability, it is less clear how well the specific pattern in the trend, i.e., the southward intensification of negative SST trend, is associated with them. The SST trends inferred from the regression coefficients and the trends in PDO and NPGO are comparable in the southern 6 buoys and the northern 6 buoys (Table 3). This is unlikely to explain the more than 70% increase in observed trend values from north to south. Similarly, the analysis of

Table 3. The Simultaneous Regression Coefficients (°C per Unit Index Change) of the JJA Buoy SST (°C) Averaged Over All 12 Buoys, the Northern 6 Buoys, and the Southern 6 Buoys Against the PDO and NPGO Indices[a]

	PDO		NPGO	
	Regression Coefficients	Inferred Trend	Regression Coefficients	Inferred Trend
All 12 buoys	+0.88	−0.42	−0.69	−0.29
Northern 6 buoys	+0.87	−0.41	−0.73	−0.30
Southern 6 buoys	+0.90	−0.42	−0.66	−0.27

[a]Also shown are the inferred trend values (°C $decade^{-1}$) obtained by multiplying the regression coefficients by the trend in each index in 1980–2010 shown in Figures 6a and 6c.

near-coast wind stress curl shows no significant regression coefficients against these indices (not shown), suggesting the trend in the near-coast curl is not significantly associated with the large-scale climate patterns either. Whether wind stress curls are independent of the direct influences of large-scale forcings, indirectly modulated by them via coastal topography, and/or associated with anthropogenic greenhouse gases forcings [*Bakun*, 1990] needs modeling and further study.

6. Summary and Discussions

[26] This study presents observational evidence of intensified coastal upwelling in the U.S. West Coast since the 1980s. NDBC coastal buoys suggest that the entire Oregon-California coastal SST has been declining at -0.19°C decade^{-1}, which is consistent with the analysis of NOAA SST data as well as previous studies [e.g., *García-Reyes and Largier*, 2010]. Furthermore, a significant cooling trend is observed that manifests itself more strongly over the southern part of the California-Oregon Coast than the northern part.

[27] The trend pattern in coastal SST is due to two different wind-driven Ekman processes acting independently in the north and south, rather than due to surface heat flux and wind-induced mixing. North of Pt. Reyes, the intensified along-shore wind stress is responsible for stronger offshore Ekman transport, since both the trend and the co-variability (i.e., a positive correlation) in meridional wind and SST are consistent with the conventional description of coastal upwelling. Off the southern coast, variability in meridional wind is negligibly correlated with that of SST, and the trends are of opposite signs. Curl-driven Ekman pumping, often associated with topographically forced wind stress curls, appears to be a dominant player in the trend in offshore upwelling transport. While the coast-wide cooling trend is highly associated with the large-scale coupled ocean-atmosphere phenomena, none predicts the specific trend patterns both in upwelling and wind stress curls. Further modeling study is necessary to elucidate the relative role of direct and indirect influences of remote forcings and the local wind stress curls in the observed trend and pattern in upwelling.

[28] In a future study, the alongshore advection of upwelled water from the north needs to be examined to see if it could contribute to the SST trend pattern. Figure 1 suggests an increased cross-shore SST gradient, which would favor a stronger southward geostrophic current advecting the upwelled water southward. This possibility cannot be tested in the present study however, due to lack of long-term high-resolution ocean current data.

[29] Finally, the buoy-measured temperature trends, while consistent with the study by *García-Reyes and Largier* [2010], are in marked contrast to findings by *Roemmich* [1992] and *Bograd and Lynn* [2003] based on the California Cooperative Oceanic Fisheries Investigations (CalCOFI) hydrography data. These authors observed a significant upper ocean warming near Pt. Conception and in SCB in 1950–1991 and 1950–1999 respectively, with the warming being associated with a deepening thermocline, increasing stratification and declining zooplankton [*Roemmich and McGowan*, 1995; *McGowan et al.*, 2003]. *Di Lorenzo et al.* [2005] further suggest that most of this observed warming in 1950–1999 can be explained by decadal variations in the PDO-driven surface heat flux and horizontal advection. In contrast, *Narayan et al.* [2010] reported, from the same CalCOFI data set [*Bograd et al.*, 2003], that compared to the offshore area (e.g., station numbers between 80 and 52), the near-coast SST and upper 100-m temperature east of station number 52 both have been significantly cooling from 1949 through 2006 [see *Narayan et al.*, 2010, Figure 8]. There is evidence that the observed trends in upwelling-favorable winds [*Bakun*, 1990; *Schwing and Mendelssohn*, 1997] would cause a decreasing trend in SST through upwelling [*Snyder et al.*, 2003; *Auad et al.*, 2006]. The warming trends are consistent with the role of PDO-modulated surface heat flux and associated stratification changes, while the cooling trend highlights the role of wind-driven upwelling. What actually causes such conflicting results from data and models, and how the different data stratifications (e.g., geographical areas: near-coast versus offshore, northern versus southern California) and modeling approaches (e.g., global versus regional and forced versus coupled) contribute to this, is not clear. Considering the strong association of the trend estimate with the climate indices (Figure 6), the different periods of analysis used in these studies could be at least partially responsible for the discrepancies in the sign of the trend. In order to clarify the dependence of short-term trend to natural climate variability and anthropogenic change, one would need to use a high-resolution regional coupled climate model that represents the small-scale upwelling processes in the context of large-scale climate variability and change. Of course, clarifying the processes that control past changes in the coastal climate is necessary for improved understanding of the range of possible future climate changes at the regional-to-local scale.

[30] **Acknowledgments.** H.S. acknowledges the WHOI supports from the Coastal Research Fund in Support of Scientific Staff, the Penzance Endowed Fund in Support of Assistant Scientists, and the Andrew W. Mellon Foundation Endowed Fund for Innovative Research. K.B. and C.E. acknowledge support by the National Science Foundation through grants OCE-1059632 and OCE 1061434. H.S. also thanks Arthur J. Miller, Young-Oh Kwon, and Jong Jin Park for their insightful comments and discussions. Authors finally wish to thank three anonymous reviewers for their comments and suggestions, which substantially improved the manuscript.

References

Auad, G., A. J. Miller, and E. Di Lorenzo (2006), Long-term forecast of oceanic conditions off California and their biological implications, *J. Geophys. Res.*, *111*, C09008, doi:10.1029/2005JC003219.

Bakun, A. (1990), Global climate change and intensification of coastal ocean upwelling, *Science*, *247*, 198–201, doi:10.1126/science.247.4939.198.

Bakun, A., and C. Nelson (1991), The seasonal cycle of wind-stress curl in subtropical eastern boundary current region, *J. Phys. Oceanogr.*, *21*, 1815–1834, doi:10.1175/1520-0485(1991)021<1815:TSCOWS>2.0.CO;2.

Bakun, A., and S. J. Weeks (2008), The marine ecosystem off Peru: What are the secrets of its sherry productivity and what might its future hold?, *Prog. Oceanogr.*, *79*, 290–299, doi:10.1016/j.pocean.2008.10.027.

Bakun, A., D. B. Enfield, A. Redondo-Rodriguez, and S. J. Weeks (2010), Greenhouse gas, upwelling-favorable winds, and the future of coastal ocean upwelling ecosystems, *Global Change Biol.*, *16*, 1213–1228, doi:10.1111/j.1365-2486.2009.02094.x.

Beardsley, R. C., C. E. Dorman, C. A. Friehe, L. K. Rosenfeld, and C. D. Winant (1987), Local atmospheric forcing during the Coastal Ocean Dynamics Experiment. 1. A description of the marine boundary layer and atmospheric conditions over a northern California upwelling region, *J. Geophys. Res.*, *92*, 1467–1488, doi:10.1029/JC092iC02p01467.

Bograd, S. J., and R. J. Lynn (2003), Long-term variability in the southern California Current System, *Deep Sea Res., Part II*, *50*, 2355–2370, doi:10.1016/S0967-0645(03)00131-0.

Bograd, S. J., D. A. Checkley Jr., and W. S. Wooster (2003), CalCOFI: A half century of physical, chemical, and biological research in the California Current System, *Deep Sea Res., Part II*, *50*, 2349–2353, doi:10.1016/S0967-0645(03)00122-X.

Bograd, S. J., I. Schroeder, N. Sarkar, X. Qiu, W. J. Sydeman, and F. B. Schwing (2009), Phenology of coastal upwelling in the California Current, *Geophys. Res. Lett.*, *36*, L01602, doi:10.1029/2008GL035933.

Brink, K. H. (1983), The near-surface dynamics of coastal upwelling, *Prog. Oceanogr.*, *12*, 223–257, doi:10.1016/0079-6611(83)90009-5.

Capet, X. J., P. Marchesiello, and J. C. McWilliams (2004), Upwelling response to coastal wind profiles, *Geophys. Res. Lett.*, *31*, L13311, doi:10.1029/2004GL020123.

Castelao, R. M., and J. A. Barth (2006), Upwelling around Cabo Frio, Brazil: The importance of wind stress curl, *Geophys. Res. Lett.*, *33*, L03602, doi:10.1029/2005GL025182.

Chenillat, F., P. Rivière, X. Capet, E. Di Lorenzo, and B. Blanke (2012), North Pacific Gyre Oscillation modulates seasonal timing and ecosystem functioning in the California Current upwelling system, *Geophys. Res. Lett.*, *39*, L01606, doi:10.1029/2011GL049966.

Chhak, K., and E. Di Lorenzo (2007), Decadal variations in the California Current upwelling cells, *Geophys. Res. Lett.*, *34*, L14604, doi:10.1029/2007GL030203.

Dever, E. P., C. E. Dorman, and J. L. Largier (2006), Surface boundary layer variability during upwelling off northern California, *Deep Sea Res., Part II*, *53*, 2887–2905, doi:10.1016/j.dsr2.2006.09.001.

Di Lorenzo, E., A. J. Miller, N. Schneider, and J. C. McWilliams (2005), The warming of the California Current: Dynamics and ecosystem implications, *J. Phys. Oceanogr.*, *35*, 336–362, doi:10.1175/JPO-2690.1.

Di Lorenzo, E., et al. (2008), North Pacific Gyre Oscillation links ocean climate and ecosystem change, *Geophys. Res. Lett.*, *35*, L08607, doi:10.1029/2007GL032838.

Diffenbaugh, N. S. (2005), Response of large-scale eastern boundary current forcing in the 21st century, *Geophys. Res. Lett.*, *32*, L19718, doi:10.1029/2005GL023905.

Diffenbaugh, N. S., M. A. Snyder, and L. C. Sloan (2004), Could CO_2-induced land-cover feedbacks alter near-shore upwelling regimes?, *Proc. Natl. Acad. Sci. U. S. A.*, *101*, 27–32, doi:10.1073/pnas.0305746101.

Dorman, C. E. (1985), Hydraulic control of the Northern California marine layer, *Eos Trans. AGU*, *66*, 914.

Dorman, C. E., and D. Koračin (2008), Interaction of the summer marine layer with an extreme California coastal bend, *Mon. Weather Rev.*, *136*, 2894–2992, doi:10.1175/2007MWR2336.1.

Dorman, C. E., and C. D. Winant (1995), Buoy observations of the atmosphere along the west coast of the United States, 1981–1990, *J. Geophys. Res.*, *100*(C8), 16,029–16,044, doi:10.1029/95JC00964.

Edwards, K. A., D. P. Rogers, and C. E. Dorman (2002), Adjustment of the marine atmospheric boundary layer to the large-scale bend in the California coast, *J. Geophys. Res.*, *107*(C12), 3213, doi:10.1029/2001JC000807.

Enriquez, A. G., and C. A. Friehe (1995), Effect of wind stress and wind stress curl variability on coastal upwelling, *J. Phys. Oceanogr.*, *25*, 1651–1671, doi:10.1175/1520-0485(1995)025<1651:EOWSAW>2.0.CO;2.

Foreman, M. G. G., B. Pal, and W. J. Merryfield (2011), Trends in upwelling and downwelling winds along the British Columbia shelf, *J. Geophys. Res.*, *116*, C10023, doi:10.1029/2011JC006995.

García-Reyes, M., and J. Largier (2010), Observations of increased wind-driven coastal upwelling off central California, *J. Geophys. Res.*, *115*, C04011, doi:10.1029/2009JC005576.

Gutiérrez, D., et al. (2011), Coastal cooling and increased productivity in the main upwelling zone off Peru since the mid-twentieth century, *Geophys. Res. Lett.*, *38*, L07603, doi:10.1029/2010GL046324.

Hamilton, G. D. (1980), Data Buoy Office programs, *Bull. Am. Meteorol. Soc.*, *61*, 1012–1017, doi:10.1175/1520-0477(1980)061<1012:NDBOP>2.0.CO;2.

Holland, P. W., and R. E. Welsch (1977), Robust regression using iteratively reweighted least-squares, *Commun. Stat.*, *6*, 813–827, doi:10.1080/03610927708827533.

Huber, P. J. (1981), *Robust Statistics*, John Wiley, Hoboken, N. J., doi:10.1002/0471725250.

Huyer, A. (1983), Coastal upwelling in the California current system, *Prog. Oceanogr.*, *12*, 259–284, doi:10.1016/0079-6611(83)90010-1.

Huyer, A., and J. G. Pattullo (1972), A comparison between wind and current observations over the continental shelf off Oregon, Summer 1969, *J. Geophys. Res.*, *77*, 3215–3220, doi:10.1029/JC077i018p03215.

Kanamaru, H., and M. Kanamitsu (2007), Fifty-Seven-Year California Reanalysis Downscaling at 10 km (CaRD10) Part II: Comparison with North American Regional Reanalysis, *J. Clim.*, *20*, 5572–5592, doi:10.1175/2007JCLI1522.1.

Kanamitsu, M., and H. Kanamaru (2007), Fifty-Seven-Year California Reanalysis downscaling at 10 km (CaRD10). Part I: System detail and validation with observations, *J. Clim.*, *20*, 5553–5571, doi:10.1175/2007JCLI1482.1.

Koračin, D., C. E. Dorman, and E. P. Dever (2004), Coastal perturbations of marine layer winds, wind stress, and wind stress curl along the California and Baja California in June 1999, *J. Phys. Oceanogr.*, *34*, 1152–1173, doi:10.1175/1520-0485(2004)034<1152:CPOMWW>2.0.CO;2.

Largier, J. L., et al. (2006), WEST: A northern California study of the role of wind-driven transport in the productivity of coastal plankton communities, *Deep Sea Res., Part II*, *53*, 2833–2849, doi:10.1016/j.dsr2.2006.08.018.

Leduc, G., C. T. Herbert, T. Blanz, P. Martinez, and R. Schneider (2010), Contrasting evolution of sea surface temperature in the Benguela upwelling system under natural and anthropogenic climate forcings, *Geophys. Res. Lett.*, *37*, L20705, doi:10.1029/2010GL044353.

Macías, D., M. R. Landry, A. Gershunov, A. J. Miller, and P. J. S. Franks (2012), Climatic control of upwelling variability along the western North-American coast [online], *PLoS ONE*, *7*, e30436, doi:10.1371/journal.pone.0030436.

Mantua, N. J., and S. R. Hare (2002), The Pacific Decadal Oscillation, *J. Oceanogr.*, *58*, 35–44, doi:10.1023/A:1015820616384.

Mantua, N. J., S. R. Hare, Y. Zhang, J. M. Wallace, and R. C. Francis (1997), A Pacific interdecadal climate oscillation with impacts on salmon production, *Bull. Am. Meteorol. Soc.*, *78*, 1069–1079, doi:10.1175/1520-0477(1997)078<1069:APICOW>2.0.CO;2.

Marchesiello, P., J. C. McWilliams, and A. Shchepetkin (2003), Equilibrium structure and dynamics of the California Current System, *J. Phys. Oceanogr.*, *33*, 753–783, doi:10.1175/1520-0485(2003)33<753:ESADOT>2.0.CO;2.

McGowan, J., S. Bograd, R. J. Lynn, and A. J. Miller (2003), The biological response to the 1977 regime shift in the California Current, *Deep Sea Res., Part II*, *50*, 2567–2582, doi:10.1016/S0967-0645(03)00135-8.

McGregor, H. V., M. Dima, H. W. Fischer, and S. Mulitza (2007), Rapid 20th-century increase in coastal upwelling off northwest Africa, *Science*, *315*, 637–639, doi:10.1126/science.1134839.

Mendelssohn, R., and F. B. Schwing (2002), Common and uncommon trends in SST and wind stress in the California and Peru–Chile current systems, *Prog. Oceanogr.*, *53*, 141–162, doi:10.1016/S0079-6611(02)00028-9.

Mesinger, F., et al. (2006), North American Regional Reanalysis, *Bull. Am. Meteorol. Soc.*, *87*, 343–360, doi:10.1175/BAMS-87-3-343.

Mestas-Nuñez, A. M., and A. J. Miller (2006), Interdecadal variability and climate change in the eastern tropical Pacific: A review, *Prog. Oceanogr.*, *69*, 267–284, doi:10.1016/j.pocean.2006.03.011.

Miller, A. J., D. R. Cayan, T. P. Barnett, N. E. Graham, and J. M. Oberhuber (1994), Interdecadal variability of the Pacific Ocean: Model response to observed heat flux and wind stress anomalies, *Clim. Dyn.*, *9*, 287–302, doi:10.1007/BF00204744.

Narayan, N., A. Paul, S. Mulitza, and M. Schulz (2010), Trends in coastal upwelling intensity during the late 20th century, *Ocean Sci. Discuss.*, *7*, 335–360, doi:10.5194/osd-7-335-2010.

Nykjær, L., and L. Van Camp (1994), Seasonal and interannual variability of coastal upwelling along northwest Africa and Portugal from 1981 to 1991, *J. Geophys. Res.*, *99*(C7), 14,197–14,207, doi:10.1029/94JC00814.

Pedlosky, J. (1978), A nonlinear model of the onset of upwelling, *J. Phys. Oceanogr.*, *8*, 178–187, doi:10.1175/1520-0485(1978)008<0178:ANMOTO>2.0.CO;2.

Pickett, M. H., and J. D. Paduan (2003), Ekman transport and pumping in the California Current based on the U.S. Navy's high-resolution atmospheric model (COAMPS), *J. Geophys. Res.*, *108*(C10), 3327, doi:10.1029/2003JC001902.

Reynolds, R. W., T. M. Smith, C. Liu, D. B. Chelton, K. S. Casey, and M. G. Schlax (2007), Daily high-resolution-blended analyses for sea surface temperature, *J. Clim.*, *20*, 5473–5496, doi:10.1175/2007JCLI1824.1.

Roemmich, D. (1992), Ocean warming and sea-level rise along the southwest United States coast, *Science*, *257*, 373–375, doi:10.1126/science.257.5068.373.

Roemmich, D., and J. McGowan (1995), Climatic warming and the decline of zooplankton in the California Current, *Science*, *267*, 1324–1326, doi:10.1126/science.267.5202.1324.

Rykaczewski, R. R., and D. M. Checkley Jr. (2008), Influence of ocean winds on the pelagic ecosystem in upwelling regions, *Proc. Natl. Acad. Sci. U. S. A.*, *105*, 1965–1970, doi:10.1073/pnas.0711777105.

Schwing, F. B., and R. Mendelssohn (1997), Increased coastal upwelling in the California Current System, *J. Geophys. Res.*, *102*, 3421–3438, doi:10.1029/96JC03591.

Schwing, F. B., T. Murphree, and P. M. Green (2002), The Northern Oscillation Index (NOI): A new climate index for the northeast Pacific, *Prog. Oceanogr.*, *53*, 115–139, doi:10.1016/S0079-6611(02)00027-7.

Smith, R. L. (1968), Upwelling, *Oceanogr. Mar. Biol.*, *6*, 11–46.

Snyder, M. A., L. C. Sloan, N. S. Diffenbaugh, and J. L. Bell (2003), Future climate change and upwelling in the California Current, *Geophys. Res. Lett.*, *30*(15), 1823, doi:10.1029/2003GL017647.

Sutton, R. T., B. Dong, and J. M. Gregory (2007), Land/sea warming ratio in response to climate change: IPCC AR4 model results and comparison with observations, *Geophys. Res. Lett.*, *34*, L02701, doi:10.1029/2006GL028164.

Sverdrup, H. U. (1937), On the process of upwelling, *J. Mar. Res.*, *1*, 155–164.

Trenberth, K. E., and J. W. Hurrell (1994), Decadal atmosphere-ocean variations in the Pacific, *Clim. Dyn.*, *9*, 303–319, doi:10.1007/BF00204745.

van Geen, A., S. N. Luoma, C. C. Fuller, R. Anima, H. E. Clifton, and S. Trumbore (1992), Evidence from Cd/Ca ratios in foraminifera for greater upwelling off California 4,000 years ago, *Nature*, *358*, 54–56, doi:10.1038/358054a0.

von Storch, H., H. Langenberg, and F. Feser (2000), A spectral nudging technique for dynamical downscaling purposes, *Mon. Weather Rev.*, *128*, 3664–3673, doi:10.1175/1520-0493(2000)128<3664:ASNTFD>2.0.CO;2.

Winant, C. D., C. E. Dorman, C. A. Friehe, and R. Beardsley (1988), The marine layer off northern California: An example of supercritical channel flow, *J. Atmos. Sci.*, *45*, 3588–3605, doi:10.1175/1520-0469(1988)045<3588:TMLONC>2.0.CO;2.

Worley, S. J., S. D. Woodruff, R. W. Reynolds, S. J. Lubker, and N. Lott (2005), ICOADS release 2.1 data and products, *Int. J. Climatol.*, *25*, 823–842, doi:10.1002/joc.1166.

Yoshida, K. (1955), Coastal upwelling off the California coast, *Rec. Oceanogr. Works Jpn.*, *2*(2), 8–20.

Yu, L., and R. A. Weller (2007), Objectively analyzed air-sea heat fluxes (OAFlux) for the global ice-free oceans, *Bull. Am. Meteorol. Soc.*, *88*, 527–539, doi:10.1175/BAMS-88-4-527.